Biosensors and Bioelectronics 151 (2020) 111973

Contents lists available at ScienceDirect

Biosensors and Bioelectronics

journal homepage: http://www.elsevier.com/locate/bios

One step preparation of CN-WS_2 nanocomposite with enhanced photoactivity and its application for photoelectrochemical detection of 5-formylcytosine in the genomic DNA of maize seedling

Fei Li, Yunlei Zhou **, Siyu Wang, Huanshun Yin *, Yan Chen, Huiyun Luo, Shiyun Ai

College of Chemistry and Material Science, Shandong Agricultural University, Taian, 271018, PR China

ARTICLE INFO

Keywords:
Photoelectrochemical biosensor
DNA formylation
CN-WS_2 composite
$ZnFe_2O_4$ artificial mimic enzyme
Eco-toxicological effect

ABSTRACT

Carbon nitride and WS_2 nanocomposite (CN-WS_2) with excellent photoelectric activity was prepared by one-step thermal polymerization. By the new strategy of simultaneously loading C and N elements on pure WS_2, the formation of CN-WS_2 brings high mobility, ultra-fast charge carrier separation and transport, and slows down the recombination rate of electrons and holes. Then, a novel photoelectrochemical biosensor was constructed for 5-formylcytosine detection based on CN-WS_2 composite, aldehyde reaction probe (ARP) and $ZnFe_2O_4$, where CN-WS_2 composite was employed as photoactive material, ARP was used as 5-formylcytosine capture reagent, and $ZnFe_2O_4$ was adopted as artificial mimic enzyme. Under the catalysis effect of $ZnFe_2O_4$, 4-chloro-1-naphthol was quickly oxidized by H_2O_2 to produce the insoluble substance of benzo-4-chlorohexadienone, which would be deposited on the electrode surface and caused a decreased PEC response. Under optimal experimental conditions, the biosensor showed low detection limit of 3 pM. This method can also discriminate 5-formylcytosine with other cytosine derivatives. More importantly, the applicability of this method was demonstrated by assessing the effect of antibiotics on the content of 5-formylcytosine in the root, stem and leave of maize seedlings.

1. Introduction

Recently, DNA formylation modification has become the focus of attention in the field of nucleic acid chemical biology. In 2011, 5-formylcytosine (5fC) was first discovered in mouse embryonic stem cells (mESCs) as an important epigenetic modification molecule (Pfaffeneder et al., 2011). After that, 5fC has also been found in many cells and tissues, such as brain tissue. Studies have shown that 5fC not only participates in the differentiation of stem cells, but also is related to alterations in the structure of the DNA double helix and protein identification (Dietzsch et al., 2018). 5fC also involves DNA demethylation process, where 5-methylcytosine (5-mC) is first oxidized to produce 5-hydroxymethylcytosine (5hmC) by the TET-family dioxygenases, and then 5hmC is further oxidized to be 5-formylcytosine (Samanta et al., 2016). To further comprehensive understand the biological functions of 5fC, sensitive and selective technique is needed. However, the content of 5fC is less than 1/10 of the 5hmC content, where 5hmC content in genomic DNA of mammalian cells can be as low as 0.0004% of cytosine (Wang et al., 2018b). Therefore, due to the low abundance of 5fC content, the detection of 5fC is faced severe challenges, which requires a highly sensitive detection method.

In the past few years, significant progress has been made in the qualitative and quantitative detection of 5fC (Wang et al., 2019g; Xia et al., 2015). To the best of our knowledge, there are currently three commonly methods for labeling and recognizing 5fC, including mass spectrometry (Iwan et al., 2017; Tang et al., 2014), sequencing (Booth et al., 2014), and fluorescent labeling (Liu et al., 2017). Due to the inherent selectivity and sensitivity of these detection methods, the detection of 5fC can be successfully realized, but there are inherent limitations, such as the need for sophisticated instruments and the need for professional operation, expensive cost, and not easy to achieve miniaturization. Therefore, it is imperative to develop new 5fC detection method with simple operation, high sensitivity and excellent specificity.

In recent years, photoelectrochemical (PEC) analysis has become increasingly important for people healthy living, environmental testing, and biomedical applications due to the advantages of low background interference, low cost, simple operation, inexpensive instrument, high sensitivity and miniaturization (Zhao et al., 2018). Based on these

* Corresponding author.
** Corresponding author.
E-mail addresses: zhyl@sdau.edu.cn (Y. Zhou), yinhs@sdau.edu.cn (H. Yin).

https://doi.org/10.1016/j.bios.2019.111973
Received 1 November 2019; Received in revised form 9 December 2019; Accepted 16 December 2019
Available online 19 December 2019

merits, PEC biosensors have been extensively applied for advanced detection of a variety of biomolecules, including curcumin (Peng et al., 2019), glucose (Çakıroğlu et al., 2019; Wang et al., 2019c), DNA (Sui et al., 2019b; Wang et al., 2019d), microRNA (Wang et al. 2019a, 2019b), protein (Li et al., 2017; Wen and Ju, 2016; Zhu et al., 2019), cells (Liu et al., 2018), etc. In our previous works, several kinds of PEC biosensors have also been successfully constructed for 5hmC and m^6A detection (Wang et al. 2018a, 2019f; Zhou et al., 2019). The above results indicate that the PEC biosensor is a promising platform for detecting 5fC.

In PEC sensors, the selection of photoactive material with good optical properties is one of the key factors affecting detection sensitivity. In date, two-dimensional transition metal dichalcogenide (e.g. MoS_2, WS_2, $MoSe_2$, WSe_2) have been widely applied in PEC analysis due to their excellent optical properties. Among them, WS_2 has received special attention due to narrow band gap and strong visible light absorption capacity (Lei et al., 2017). The bulk WS_2 is an indirect gap semiconductor with a gap of 1.3 eV, and as the material transitions to a single layer, its gap increases directly with increasing size. In addition, the metal W atom is bonded to the S atom through a strong covalent bond in the layer, and the layers are further superimposed by a weak van der Waals interaction (Cheng et al., 2014). However, due to its weak conductivity and the faster recombination rate of electrons and holes, the application of WS_2 is limited. To overcome these shortcomings, researchers are looking for an effective charge separation strategy to improve the photoelectric performance by coupling WS_2 with other materials. For examples, Zou et al. synthesized a multi-layer-cake WS_2/C nanocomposite by intercalation-transformation method. The WS_2/C nanocomposites exhibit good performance due to the enhanced conductivity of the interlayer carbon and the unique regular alternating structure (Zou et al., 2017). Zhao's group increased the photoexcited carrier lifetime and reduced the electron-hole recombination rate via the synthesis of N-doped WS_2 compound (Zhao et al., 2015). Inspired by those researches, we propose a new strategy to simultaneously load both C and N elements on pure WS_2 (CN-WS_2), so that the formation of CN-WS_2 brings high mobility, ultra-fast charge carrier separation and transportation, slows down the recombination rate of electrons and holes. Notably, this increases the absorption efficiency of light and is critical to the successful integration of WS_2 into PEC biosensors.

As an effective signal inhibition model, biocatalytic precipitation (BCP) has been combined with PEC technology with increased detection sensitivity (Zhang et al., 2019), where BCP refers to the process of forming insoluble product on the modified electrode surface under enzyme catalysis. The formed insulating layer can greatly change the interface electron transfer characteristics and thus lead to a significant effect on the photocurrent (Gong et al., 2016b; Zhuang et al., 2015). However, natural enzymes often have problems such as expensive cost, poor stability, difficulty in storage, and variability, which limits their application. In order to overcome these shortcomings, in recent years, various artificial mimicking enzymes have been prepared and alternatively replaced the application of natural enzyme (Gong et al., 2016a; Li et al., 2018). $ZnFe_2O_4$, as an artificial mimetic enzyme, have intrinsic peroxide activity, which can mimic the catalytic property of horseradish peroxidase (HRP) (Wang et al., 2019e). Moreover, $ZnFe_2O_4$ not only have the advantages of low cost, excellent catalytic efficiency and good stability, but also easy separation, surface functionalization, and simple preparation method (Xiao et al., 2018). Therefore, $ZnFe_2O_4$ can be used in combination with BCP and photoelectrochemistry for 5fC detection.

Herein, carbon nitride and WS_2 nanocomposite (CN-WS_2) was firstly prepared by one-step thermal polymerization, and its morphology, structure and optical properties were investigated in detail. Based on the excellent photoactivity of CN-WS_2, a novel PEC biosensor was constructed for 5fC detection, where CN-WS_2 was employed as the photoelectric material, the aldehyde reaction probe (ARP) was used as 5fC recognition reagent, and $ZnFe_2O_4$ was employed as signal quenching unit. To evaluate the practical application of the developed method, the effect of antibiotics on the content of 5fC in the root, stem and leave of maize seedlings were investigated, and the results were compared with ELISA method.

2. Experimental section

2.1. Regents and instruments

See Supporting Information.

2.2. Synthesis of CN-WS_2, $ZnFe_2O_4$ and AuNPs

See Supporting Information.

2.3. Biosensor fabrication

The pretreatment of ITO conductive glass was carried out as previously reported study (Wang et al., 2017). Next, 40 μL of 3 mg/mL CN-WS_2 dispersion was dropped onto the bare ITO electrode surface and dried under the irradiation of infrared lamp. The unimmobilized CN-WS_2 was removed by rinsing the electrode with deionized water for three times. The prepared electrode was denoted as CN-WS_2/ITO. Then, 40 μL of 13 nM AuNPs was dropped on CN-WS_2/ITO surface and dried under the irradiation of infrared lamp. The obtained electrode was named as AuNPs/CN-WS_2/ITO. After rinsed with deionized water for three times, the electrode was incubated with 40 μL of 0.1 mg/mL streptavidin solution (SA) for 100 min in a humidified incubator at 37 °C. The obtained SA/AuNPs/CN-WS_2/ITO electrode was rinsed three times with washing buffer to remove unreacted SA. Subsequently, 40 μL of 0.1 mM MCH was added to the above obtained modified electrode and was incubated for 0.5 h in order to block unreacted AuNPs. After rinsing three times with washing buffer, 40 μL of 10 μg/mL aldehyde reaction probe (ARP) was dropped onto the above electrode and placed in a humidified incubator at 37 °C for 120 min. The obtained electrode (ARP/SA/AuNPs/CN-WS_2/ITO) was then rinsed three times with washing buffer, followed by 40 μL of 5fC (1 nM) was deposited on the electrode and incubated for 120 min. The prepared electrode was denoted as 5fC/ARP/SA/AuNPs/CN-WS_2/ITO. Subsequently, 40 μL of 3 mg/mL $ZnFe_2O_4$ was dropped onto the electrode surface and incubated for 120 min at room temperature. This electrode was further incubated with 40 μL of 10 mM Tris-HCl-AA solution containing 10 mM 4-CN and 0.15 mM H_2O_2 for 30 min. Finally, the electrode was rinsed with washing buffer for three times. The obtained electrode was denoted as $ZnFe_2O_4$/5fC/ARP/SA/AuNPs/CN-WS_2/ITO.

3. Results and discussion

3.1. Detection strategy

In this work, a sensitive and selective PEC method was developed for 5fC detection. For the first time, CN-WS_2 was synthesized and employed as photoactive material in the PEC method. With the doping of C and N, the photoactivity of WS_2 was improved greatly, which could also increase the sensitivity of this method. As shown in Scheme 1, CN-WS_2 and AuNPs were successively modified on the bare ITO electrode surface. Then, base on the formation of Au–N bond between AuNPs and streptavidin, streptavidin was assembled on the electrode surface. After blocking the activity of AuNPs with MCH, APR was further modified on the electrode surface through the specific interaction between atreptavidin and biotin (where one biotin molecule was labeled in the structure of ARP). Afterwards, according to the specifically chemical reaction between ARP and the formyl of 5fC, 5fC was selectively recognized and modified on the electrode surface. The application of ARP can effectively discriminate 5fC with 5mC, 5hmC and 5caC. Finally, $ZnFe_2O_4$ was captured on the electrode surface through the interaction between the phosphate group of immobilized 5fC and Zn^{2+} (Sui et al., 2019a). As an

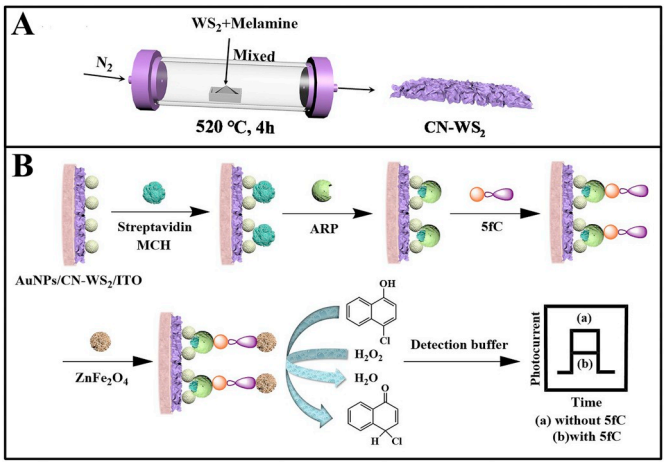

Scheme 1. Schematic illustration of preparation process of CN-WS_2 (A) and the proposed $ZnFe_2O_4$ induced BCP-based PEC biosensor construction process (B).

artificial mimic enzyme, $ZnFe_2O_4$ has the catalytic activity of HRP, which can accelerate the oxidation of 4-CN by H_2O_2 to form insulating film of benzo-4-chlorohexadienone on the electrode surface. It can hinder the transmission of electron donor (AA), and increase the recombination of photogenerated electron and hole. Therefore, the PEC response of the electrode decreases. Based on the linear relationship between PEC response and the concentration of 5fC, 5fC can be quantitatively detected.

3.2. Characterization of materials

The prepared CN-WS_2 composites were characterized by SEM, TEM, EDS mapping, XRD and FT-IR. Fig. 1A presents the SEM image of pure WS_2 with plate-like structure. After melamine and WS_2 was calcined in nitrogen, some irregular small CN nanosheets were loaded on the surface of WS_2 (Fig. 1B). Under high resolution, the CN nanosheets and WS_2 are in intimate contact (Fig. 1C). Fig. 1D shows the TEM image of CN-WS_2, indicating that CN is well distributed on the surface of WS_2. The HRTEM image (inset of Fig. 1D) shows lattice fringe with a spacing of 0.27 nm, which can be assigned to the (100) plane of WS_2, while CN has insufficient crystallinity and therefore no corresponding lattice spacing was found. In addition, the corresponding EDS mapping spectrum of CN-WS_2 was investigated. As shown in Fig. 1E and F, the results demonstrated the C, N, W, S elements in the composite, which further clarifies the coupling of WS_2 and CN nanosheets. XRD analysis was recorded to illuminate the phase structures of the prepared CN-WS_2 composite. As shown in Fig. 1G, the XRD pattern of CN-WS_2 is directed to the hexagonal phase WS_2 (JCPDS card no. 85–1068) (Sang et al., 2015). More specifically, after calcination, the crystallinity of WS_2 is also improved, and the peak intensity is increased. No diffraction peak associated with CN is observed in the image, which might be caused by the poor crystallinity of CN. CN-WS_2 was further characterized by FT-IR (Fig. 1H). Compared with pure WS_2, the broad bands in the 3424 cm^{-1} can be attributed to the typical stretching vibrations of N–H in the CN-WS_2 composite. In addition, the band belonging to the stretching vibrations of C–N or C═N heterocycle were at about 804 cm^{-1} and 1000–1700 cm^{-1}. The absorption peaks of CN-WS_2 at about 885 cm^{-1} were originated from the deformation mode of N–H. Therefore, the CN nanosheets were successfully generated in situ on the surface of the WS_2. The characterization of AuNPs and $ZnFe_2O_4$ was illustrated in Fig. 2 and the corresponding description was presented in Supporting Information.

To prove that CN-WS_2 composite is significantly different from g–C_3N_4–WS_2, we tested the photocurrent response of WS_2, g-C_3N_4, g–C_3N_4–WS_2 and CN-WS_2 samples. As can be seen from Fig. 3A, the PEC response of WS_2 is 0.52 μA, g-C_3N_4 is 0.21μA, g–C_3N_4–WS_2 is 1.06 μA, while the PEC response of CN-WS_2 composite is 6.12 μA, photocurrent response is significantly higher than g–C_3N_4–WS_2. Further, in order to elucidate the effect of CN coupling on WS_2 photoactivity, the PEC response of WS_2 and CN-WS_2 was investigated. As shown in Fig. 3B, both WS_2 and CN-WS_2 could respond quickly during repeated on/off cycles of visible light illumination, and a stable, reproducible photocurrent response is observed. WS_2 exhibits a weak photocurrent response due to the rapid recombination of photogenerated electron and hole. However, CN-WS_2 exhibits a strong photocurrent intensity (approximately 17 times to that of the WS_2), indicating higher separation and migration efficiency of photogenerated carriers, thereby improving optoelectronic performance.

To investigate the effect of CN on the conductibility of WS_2, EIS measurement and fluorescence spectrum analysis were performed. Fig. 3C presents the Nyquist curve of GCE, WS_2/GCE and CN-WS_2/GCE. For GCE, only a small semi-circle was observed, indicating a small interface electron transfer resistance (R_{et}). The R_{et} for WS_2/GCE increased greatly, which demonstrated the weak conductivity and low electron migration rate of WS_2. However, after modified with CN, the R_{et} value decreased significantly. This result strongly proves that the conductivity and electron migration ability of WS_2 are greatly improved due

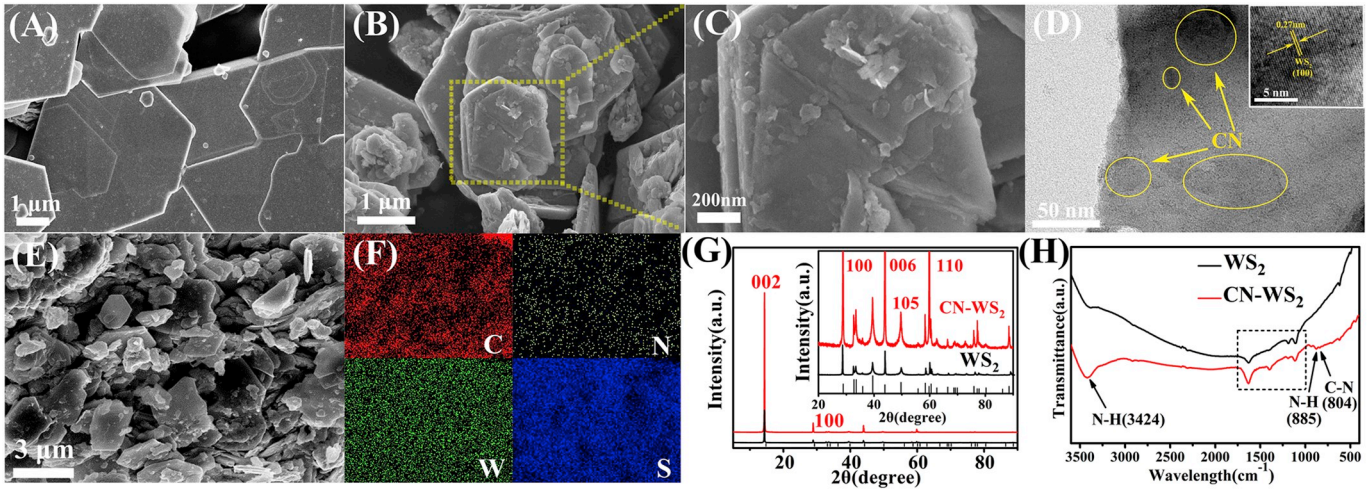

Fig. 1. (A) SEM image of pure WS_2. (B, C) Typical SEM images of CN-WS_2 composite under different magnifications. (D) TEM image of CN-WS_2 (inset of (D) is the HRTEM of CN-WS_2). (E, F) SEM image and corresponding the element mappings of C, N, W, S for CN-WS_2 composite. (G) XRD patterns of WS_2 and CN-WS_2. (H) FT-IR spectra of WS_2 and CN-WS_2.

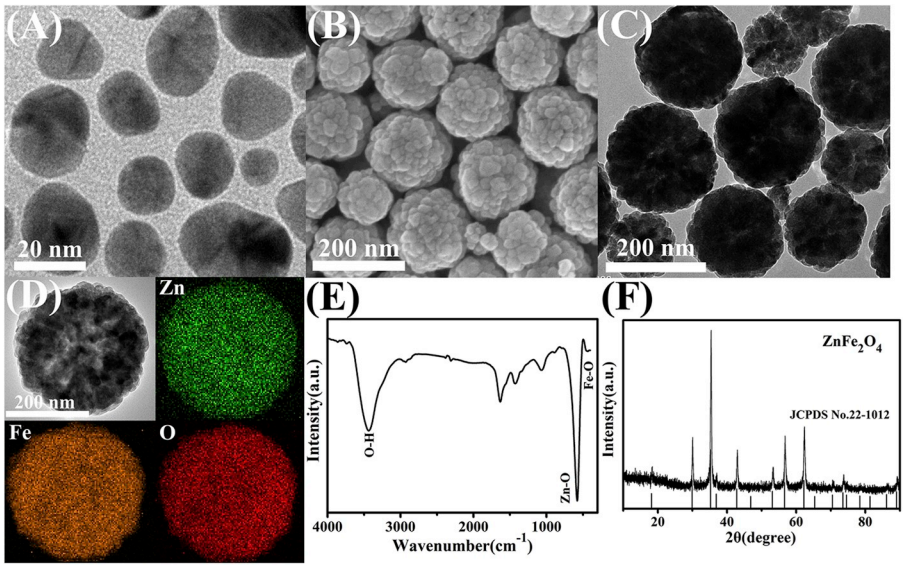

Fig. 2. (A) TEM image of AuNPs. SEM (B) and TEM (C) images of $ZnFe_2O_4$. (D) TEM image and the EDS mapping of a single $ZnFe_2O_4$ nanosphere. (E) FT-IR of $ZnFe_2O_4$. (F) XRD patterns of $ZnFe_2O_4$.

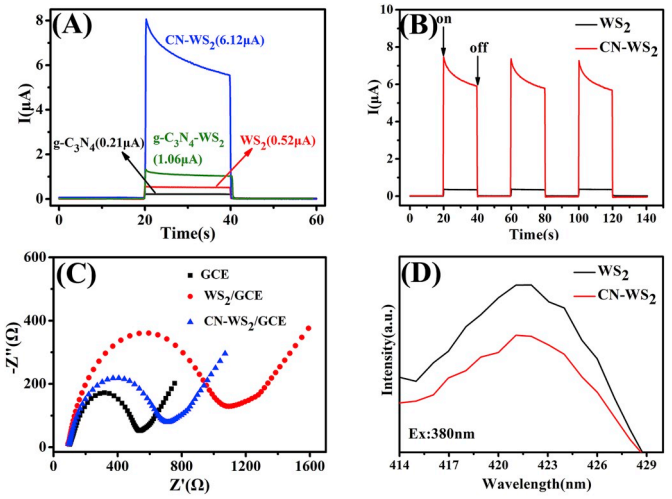

Fig. 3. (A) Photocurrent response of WS_2, g-C_3N_4, g–C_3N_4–WS_2, CN-WS_2 samples with visible light. (B) Photocurrent response of WS_2 and CN-WS_2 with visible light on/off cycles at -0.2 V. (C) Nyquist plot for different electrodes in 10 mM Tris-HCl containing 5 mM $K_3[Fe(CN)_6]/K_4[Fe(CN)_6]$ (1:1) and 0.1 M KCl. (D) PL emission spectra of WS_2 and CN-WS_2 at an excitation wavelength of 380 nm.

to the introduction of C element, which accelerates the electron transfer and transportation at the contact interface and increases the conductivity of the composite.

Fig. 3D depicts the PL spectrum of WS_2 and CN-WS_2 with an excitation wavelength of λ = 380 nm. It can be seen that the higher PL intensity was obtained on WS_2, owing to the rapid recombination of photoinduced electrons and holes. Moreover, the CN-WS_2 sample displayed the lower PL intensity, which indicated a delay in recombination rate of photogenerated charges (Zou et al., 2018). It is evident that the introduction of CN can effectively promote the charge separation, and the close contact between WS_2 and CN can hinder the recombination of electrons and holes, resulting in high photoelectric activity. Therefore, based on the results from the PL spectroscopy, photocurrent response and EIS measurement, it can be reasonably concluded that the excellent photoelectric performance on CN-WS_2 is mainly attributed to the introduction of CN.

3.3. Characterization of the modified electrodes

To characterize the biosensor fabrication process and detection feasibility, the PEC response of different electrodes were recorded. As seen in Fig. 4A, CN-WS_2/ITO presents a strong photocurrent due to the improved photoactivity of CN-WS_2. As a new composite material, compared with pure WS_2, CN-WS_2 not only increases its conductivity, but also accelerates the transfer of electrons. Moreover, the introduction of N reduces the electron-hole recombination rate, resulting in lower electron hole recombination and more efficient carrier migration, thereby producing a higher and stable photocurrent. After the introduction of AuNPs, the photocurrent increases greatly (curve b). This

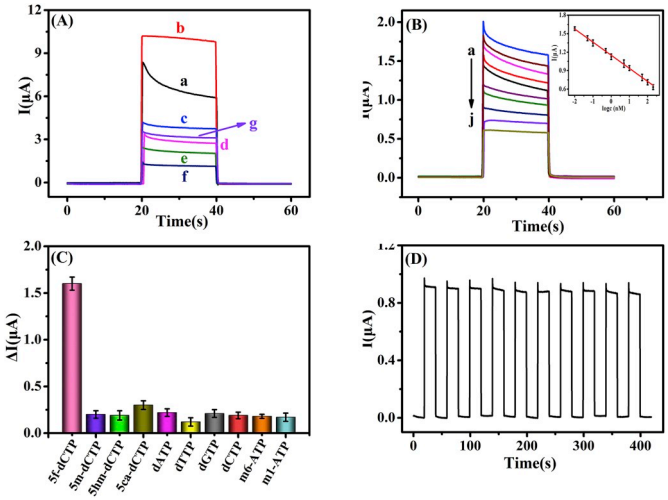

Fig. 4. (A) PEC response of different electrode in 10 mM Tris-HCl-AA solution (pH = 7.4) containing 10 mM 4-CN and 0.15 mM H_2O_2. (a) CN-WS_2/ITO, (b) AuNPs/CN-WS_2/ITO, (c) SA/AuNPs/CN-WS_2/ITO, (d) ARP/SA/AuNPs/CN-WS_2/ITO, (e) 5fC/ARP/SA/AuNPs/CN-WS_2/ITO, (f) $ZnFe_2O_4$/5fC/ARP/SA/AuNPs/CN-WS_2/ITO, (g) ARP/SA/AuNPs/CN-WS_2/ITO incubated with $ZnFe_2O_4$. (B) The photocurrent of the biosensor with different concentrations of 5f-dCTP in 10 mM Tris-HCl-AA solution (pH 7.4). (a–j): 0.01, 0.05, 0.1, 0.5, 1, 5, 10, 50, 100, 200 nM. Inset graph, a linear plot of photocurrent response versus logarithm of 5f-dCTP concentration. (C) The PEC response change of the biosensor after it was incubated with 1 nM different deoxyribonucleotides. (D) Time-based photocurrent responses of the biosensor with light on and off.

increase can be attributed to ionic resonance absorption of AuNPs, which can absorb light energy to the greatest extent, improve photogenerated electron ratio and photoelectric conversion efficiency. In addition, AuNPs can promote the separation and transfer of electrons in CN-WS_2, and also increase the electrode surface area, resulting in substantial increase in photocurrent. Curve c is the PEC response of SA/AuNPs/CN-WS_2/ITO electrode. After immobilizing streptavidin on the electrode by formation of Au–N bond, the photocurrent decreases significantly, which may be due to the increased steric hindrance of immobilized streptavidin. Moreover, streptavidin can also adsorb the visible light, which can block the visible light absorption of CN-WS_2, and result in a decrease in photocurrent. Subsequently, when ARP is further captured on SA/AuNPs/CN-WS_2/ITO surface by specific binding between avidin and biotin, the photocurrent further decreases (curve d), which can be attributed to the steric hindrance effect causing by ARP, blocking the diffusion of electron donor to electrode surface. After the modification of 5fC, the photocurrent further decreases (curve e), which can be attributed to steric hindrance effect and electrostatic repulsion effect of 5fC. After the 5fC/ARP/SA/AuNPs/CN-WS_2/ITO electrode was modified with $ZnFe_2O_4$, the photocurrent is significantly reduced to around 1.2 μA (curve f). As an artificial mimic enzyme, $ZnFe_2O_4$ can simulate the catalytic activity of HRP, accelerate 4-chloro-1-naphthol decomposition and form insulating substance benzo-4-chloroketene deposited on the surface of the electrode. As a result, the light absorption characteristics of the electrode are changed, and the transmission of electron donor is hindered, which lead to a decreased photocurrent. To determine the importance of 5f-dCTP in the capture of $ZnFe_2O_4$, a control experiment was performed. To do it,the ARP/SA/CN-WS_2/ITO electrode was firstly directly incubated with $ZnFe_2O_4$ for 120 min. Then, the PEC performance of the modified electrode was recorded (curve g) and compared with $ZnFe_2O_4$/5fC/ARP/SA/CN-WS_2/ITO (curve f). The photocurrent for curve g is much higher than that of curve f. This result demonstrates that $ZnFe_2O_4$ can be assembled on the electrode surface only in the presence of 5f-dCTP. Therefore, this biosensor is shown to be useful for the detection of 5f-dCTP.

3.4. Optimization of detection conditions

See Supporting Information.

3.5. Performance of the biosensor for 5f-dCTP detection

The PEC response of the biosensor was recorded with different concentrations of 5f-dCTP under optimal experimental conditions (See Supporting Information). As shown in Fig. 4B, when the concentration of 5f-dCTP changing from 0.01 to 200 nM, the PEC response decreases gradually. Fig. 4B inset graph shows a strong negative linear relationship between the photocurrent and the logarithm of the 5f-dCTP concentration. The linear regression equation is I (μA) = -0.21log$c$ (nM) + 1.15 ($R^2 = 0.997$), with a sensitivity of 4.6 $\mu A nM^{-1} cm^{-2}$. The limit of detection (LOD) was calculated by using the formula, LOD = 3 Sb/S (Sb: standard deviation of ten blank measurements and S: sensitivity) (Çakıroğlu and Özacar, 2018, 2019), and was calculated as 3 pM. Compared with other methods for 5fC detection, this PEC sensor exhibits a wider linear range and a relatively lower detection limit (Table S1, see Supporting Information). Although our sensitivity needs to further be improved, our method also possesses some other merits, such as enzyme-free, mild detection condition, inexpensive instrument, rapid response, simplicity operation.

Specificity is a vital indicator for new developed biosensor. To evaluate the detection specificity, 5m-dCTP, 5hm-dCTP, 5ca-dCTP, dATP, dTTP, dGTP, dCTP, m6-dATP, and m1-dATP were employed as possible interfering substances. The biosensor was then prepared as the process described in section 2.3 with different nucleotides. The photocurrent change ($\Delta I = I_2$ - I_1) was compared, where I_2 represented the photocurrent of ARP/SA/AuNPs/CN-WS_2/ITO, and I_1 represented the photocurrent of ARP/SA/AuNPs/CN-WS_2/ITO incubated with different nucleotides and $ZnFe_2O_4$ successively. As illustrated in Fig. 4C, the ΔI for 5f-dCTP is greatly higher than that for other nucleotides, indicating the good selectivity for 5fC detection.

The stability of biosensors is also an important property for biosensor. To assess it, the photocurrent of the biosensor was recorded during the light on and light off. As can be seen in Fig. 4D, the photocurrent for the 10 consecutive cycles are basically equal in magnitude and the peak shape was stable. The relative standard deviation (RSD) is 1.6%, indicating that the sensor has good stability.

3.6. Effect of antibiotic on the content of 5fC in maize issue

Antibiotic is a class of compounds with antibacterial activity. However, the antibiotic residue in animal-based food is one of the typical food safety issues and is deemed as an important health hazard owing to abuse and increasing antimicrobial resistance. However, the effect of antibiotic on plant growth, especially on crop, are seldom investigated. Thus, to further evaluate the applicability of the constructed PEC biosensor for 5fC detection in biological samples, the effects of three typical antibiotic (Amoxicillin, chloramphenicol and tobramycin, which belong to three typical kinds of antibiotic, that is β-lactams, amide alcohols and aminoglycosides, respectively) on the 5fC content in the root, stem and leave of maize seedlings were investigated. As shown in Fig. 5, the effect of the three kind of antibiotics on 5fC content are different. Amoxicillin causes the decrease of 5fC in the root, stem and leave of maize seedling. On the contrary, chloramphenicol and tobramycin lead to the increase of 5fC. These results suggest that antibiotics have greatly effect on the formation of 5fC, and different types of antibiotics have different effects on 5fC expression. These results indicate that the prepared biosensor has broad application prospects. Moreover, this study also demonstrates that 5fC might be a new biomarker for evaluating the ecotoxicological effects of antibiotics on crop.

4. Conclusions

In summary, a new photoactive material of CN-WS_2 has been successful prepared by one-step high temperature calcination method using melamine and WS_2 as raw materials. Due to the dope of C and N elements, the photoactivity and conductibility of WS_2 is improved greatly, which results in the significant increase of the PEC response of WS_2. Based on the specific recognition of ARP to formyl group, 5fC can be specific captured and detected with high sensitivity. This biosensor greatly broadened the linear range (0.01–200 nM) with a low detection limit of 3 pM (S/N = 3). Importantly, the developed PEC biosensor was successfully applied to the detection of 5fC in antibiotic-contaminated maize samples, and demonstrated that antibiotics have greatly effect on the expression level of DNA formylation. Moreover, this study might be a potential platform for investigating the ecotoxicological effects of antibiotics using 5fC as new biomarker.

Author contribution statement

Fei Li: Conceptualization, Data curation, Formal analysis, Methodology, Investigation, Roles/Writing - original draft. Yunlei Zhou: Investigation, Funding acquisition, Project administration, Resources, Supervision, Writing - review & editing. Siyu Wang: Formal analysis, Data curation, Investigation. Huanshun Yin: Investigation, Funding acquisition, Project administration, Resources, Supervision, Writing - review & editing. Yan Chen: Formal analysis, Data curation, Investigation, Validation. Huiyun Luo: Formal analysis, Data curation, Investigation, Validation. Shiyun Ai: Funding acquisition, Project administration, Supervision.

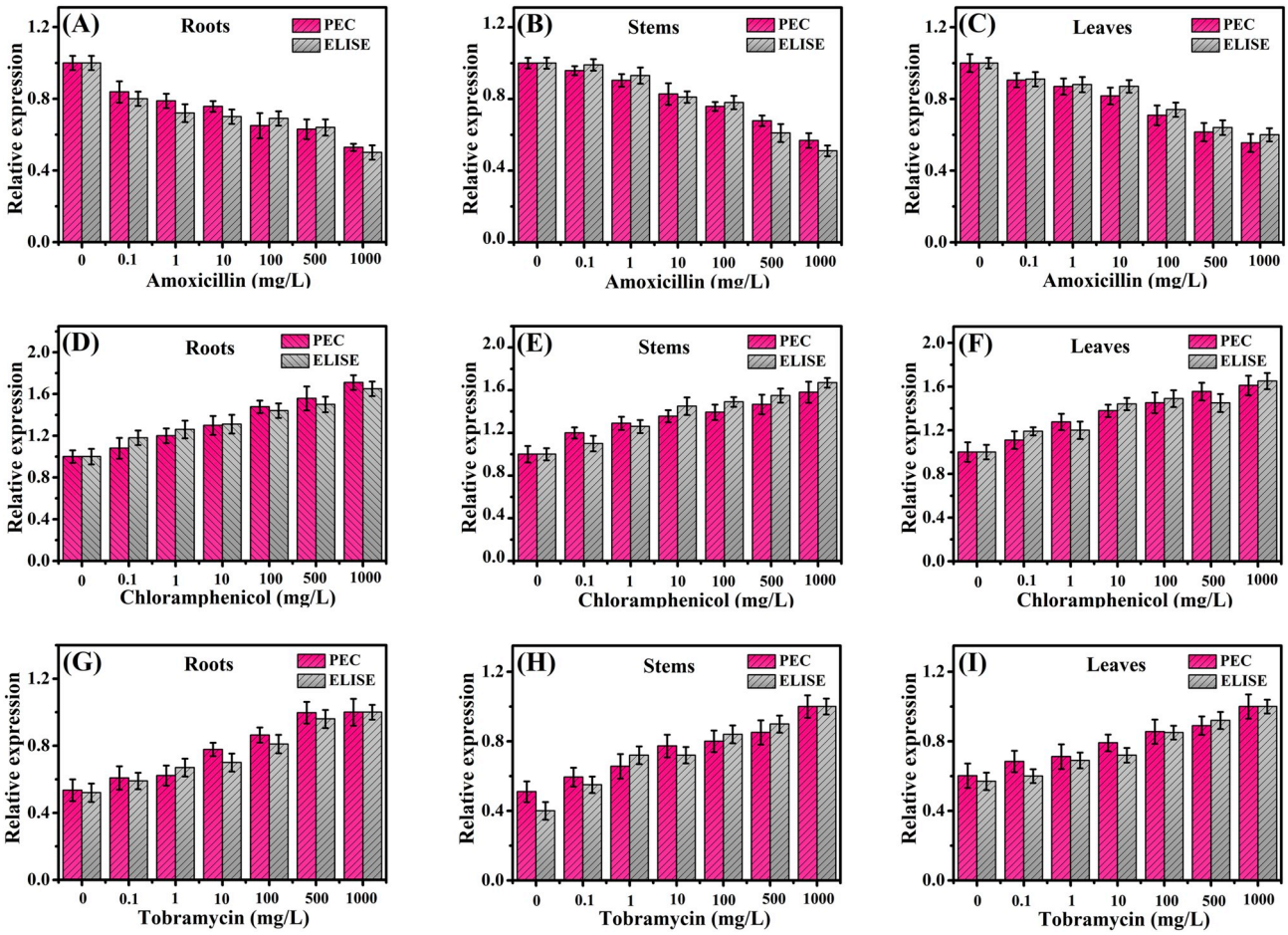

Fig. 5. Effect of amoxicillin (A–C), chloramphenicol (D–F) and tobramycin (G–I) on 5fC expression in the genomic DNA of root, stem, leave of maize seedlings.

Declaration of competing interest

The authors declare that they have no known competing financial interests or personal relationships that could have appeared to influence the work reported in this paper.

CRediT authorship contribution statement

Fei Li: Conceptualization, Data curation, Formal analysis, Methodology, Investigation, Writing - original draft. **Yunlei Zhou:** Investigation, Funding acquisition, Project administration, Resources, Supervision, Writing - review & editing. **Siyu Wang:** Formal analysis, Data curation, Investigation. **Huanshun Yin:** Investigation, Funding acquisition, Project administration, Resources, Supervision, Writing - review & editing. **Yan Chen:** Formal analysis, Data curation, Investigation, Validation. **Huiyun Luo:** Formal analysis, Data curation, Investigation, Validation. **Shiyun Ai:** Funding acquisition, Project administration, Supervision.

Acknowledgments

This work was supported by the National key research and development project of China (2018YFC1800605), Key research and development project of Shandong Province (2019GSF107023), the National Natural Science Foundation of China (21775090, 41807484, 41977345), the Natural Science Foundation of Shandong Province, China (ZR2018MB028).

Appendix A. Supplementary data

Supplementary data to this article can be found online at https://doi.org/10.1016/j.bios.2019.111973.

References

Booth, M.J., Marsico, G., Bachman, M., Beraldi, D., Balasubramanian, S., 2014. Nat. Chem. 6, 435–440.
Çakıroğlu, B., Demirci, Y.C., Gökgöz, E., Özacar, M., 2019. Sens. Actuators B Chem. 282, 282–289.
Çakıroğlu, B., Özacar, M., 2018. Biosens. Bioelectron. 119, 34–41.
Çakıroğlu, B., Özacar, M., 2019. Biosens. Bioelectron. 141, 111385.
Cheng, L., Huang, W., Gong, Q., Liu, C., Liu, Z., Li, Y., Dai, H., 2014. Angew. Chem. Int. Ed. 53, 7860–7863.
Dietzsch, J., Feineis, D., Höbartner, C., 2018. FEBS Lett. 592, 2032–2047.
Gong, L., Dai, H., Zhang, S., Lin, Y., 2016. Anal. Chem. 88, 5775–5782.
Gong, L., Dai, H., Zhang, S., Lin, Y., 2016. Anal. Chem. 88, 5775–5782.
Iwan, K., Rahimoff, R., Kirchner, A., Spada, F., Schröder, A.S., Kosmatchev, O., Ferizaj, S., Steinbacher, J., Parsa, E., Müller, M., Carell, T., 2017. Nat. Chem. Biol. 14, 72.
Lei, T., Chen, W., Huang, J., Yan, C., Sun, H., Wang, C., Zhang, W., Li, Y., Xiong, J., 2017. Adv. Energy Mater. 7, 1601843.
Li, J., Li, X., Zhao, Q., Jiang, Z., Tadé, M., Wang, S., Liu, S., 2018. Sens. Actuators B Chem. 255, 133–139.
Li, X., Zhu, L., Zhou, Y., Yin, H., Ai, S., 2017. Anal. Chem. 89, 2369–2376.
Liu, C., Wang, Y., Yang, W., Wu, F., Zeng, W., Chen, Z., Huang, J., Zou, G., Zhang, X., Wang, S., Weng, X., Wu, Z., Zhou, Y., Zhou, X., 2017. Chem. Sci. 8, 7443–7447.
Liu, S., He, P., Hussain, S., Lu, H., Zhou, X., Lv, F., Liu, L., Dai, Z., Wang, S., 2018. ACS Appl. Mater. Interfaces 10, 6618–6623.
Peng, J., Huang, Q., Liu, Y., Liu, P., Zhang, C., 2019. Sens. Actuators B Chem. 294, 157–165.
Pfaffeneder, T., Hackner, B., Truß, M., Münzel, M., Müller, M., Deiml, C.A., Hagemeier, C., Carell, T., 2011. Angew. Chem. Int. Ed. 50, 7008–7012.
Samanta, B., Seikowski, J., Höbartner, C., 2016. Angew. Chem. Int. Ed. 55, 1912–1916.
Sang, Y., Zhao, Z., Zhao, M., Hao, P., Leng, Y., Liu, H., 2015. Adv. Mater. 27, 363–369.

Sui, C., Li, F., Wu, H., Yin, H., Zhang, S., Waterhouse, G.I.N., Wang, J., Zhu, L., Ai, S., 2019. Biosens. Bioelectron. 142, 111516.
Sui, C., Wang, T., Zhou, Y., Yin, H., Meng, X., Zhang, S., Waterhouse, G.I.N., Xu, Q., Zhuge, Y., Ai, S., 2019. Biosens. Bioelectron. 127, 38–44.
Tang, Y., Xiong, J., Jiang, H.-P., Zheng, S.-J., Feng, Y.-Q., Yuan, B.-F., 2014. Anal. Chem. 86, 7764–7772.
Wang, H., Yin, H., Huang, H., Li, K., Zhou, Y., Waterhouse, G.I.N., Lin, H., Ai, S., 2018. Biosens. Bioelectron. 108, 89–96.
Wang, H., Zhang, Q., Yin, H., Wang, M., Jiang, W., Ai, S., 2017. Biosens. Bioelectron. 95, 124–130.
Wang, M., Yin, H., Zhou, Y., Meng, X., Waterhouse, G.I.N., Ai, S., 2019. Chem. Eng. J. 365, 351–357.
Wang, M., Yin, H., Zhou, Y., Sui, C., Wang, Y., Meng, X., Waterhouse, G.I.N., Ai, S., 2019. Biosens. Bioelectron. 128, 137–143.
Wang, S., Li, S., Wang, W., Zhao, M., Liu, J., Feng, H., Chen, Y., Gu, Q., Du, Y., Hao, W., 2019. Sens. Actuators B Chem. 291, 34–41.
Wang, S., Zhao, J., Zhang, Y., Yan, M., Zhang, L., Ge, S., Yu, J., 2019. Biosens. Bioelectron. 139, 111325.
Wang, X., Zhao, M., Song, Y., Liu, Q., Zhang, Y., Zhuang, Y., Chen, S., 2019. Sens. Actuators B Chem. 283, 130–137.
Wang, Y., Liu, C., Zhang, X., Yang, W., Wu, F., Zou, G., Weng, X., Zhou, X., 2018. Chem. Sci. 9, 3723–3728.
Wang, Y., Yin, H., Li, X., Waterhouse, G.I.N., Ai, S., 2019. Biosens. Bioelectron. 131, 163–170.
Wang, Y., Zhang, X., Zou, G., Peng, S., Liu, C., Zhou, X., 2019. Accounts Chem. Res. 52, 1016–1024.
Wen, G., Ju, H., 2016. Anal. Chem. 88, 8339–8345.
Xia, B., Han, D., Lu, X., Sun, Z., Zhou, A., Yin, Q., Zeng, H., Liu, M., Jiang, X., Xie, W., He, C., Yi, C., 2015. Nat. Methods 12, 1047.
Xiao, N., Liu, S.G., Mo, S., Yang, Y.Z., Han, L., Ju, Y.J., Li, N.B., Luo, H.Q., 2018. Sens. Actuators B Chem. 273, 1735–1743.
Zhang, L., Shi, X.-M., Xu, Y.-T., Fan, G.-C., Yu, X.-D., Liang, Y.-Y., Zhao, W.-W., 2019. Biosens. Bioelectron. 134, 103–108.
Zhao, W.-W., Xu, J.-J., Chen, H.-Y., 2018. Anal. Chem. 90, 615–627.
Zhao, X., Xia, C., Wang, T., Peng, Y., Dai, X., 2015. J. Alloy. Comp. 649, 357–361.
Zhou, Y., Yin, H., Sui, C., Wang, Y., Ai, S., 2019. Chem. Eng. J. 357, 94–102.
Zhu, L.-B., Lu, L., Wang, H.-Y., Fan, G.-C., Chen, Y., Zhang, J.-D., Zhao, W.-W., 2019. Biosens. Bioelectron. 140, 111349.
Zhuang, J., Lai, W., Xu, M., Zhou, Q., Tang, D., 2015. ACS Appl. Mater. Interfaces 7, 8330–8338.
Zou, J., Liu, C., Yang, Z., Qi, C., Wang, X., Qiao, Q., Wu, X., Ren, T., 2017. ChemElectroChem 4, 2232–2236.
Zou, Y., Shi, J.-W., Ma, D., Fan, Z., Cheng, L., Sun, D., Wang, Z., Niu, C., 2018. ChemSusChem 11, 1187–1197.